Molecular motor in a box: Attractors, repellers, and ratchets in chromatin

Sophie Klempahn [1], Ralf Blossey [2] and Helmut Schiessel[1,3]

[1]*Cluster of Excellence Physics of Life, TUD Dresden University of Technology, 01307 Dresden, Germany*
[2]*L'Unité de Glycobiologie Structurale et Fonctionnelle, Université de Lille, Centre National de la Recherche Scientifique UMR8576, 59000 Lille, France*
[3]*Institut für Theoretische Physik, TUD Dresden University of Technology, 01069 Dresden, Germany*

The spatiotemporal organization of eukaryotic DNA is controlled by an intricate combination of passive (thermally activated) and active (ATP-consuming) processes. Based on recent experimental insights into the mechanochemical cycle of chromatin remodelers, molecular machines that actively control nucleosome positions, we introduce a model to study the competition between active and passive mechanisms at the most basic layer of DNA packaging, the wrapping of DNA into nucleosomes. Depending on the level of remodeler activity, the positions of nucleosomes are controlled by either the bending or the stretching energy of the wrapped DNA involved. Since these energies are highly sequence dependent, DNA guides its own packaging. However, since this dependence differs for the two deformation modes, active processes can drive nucleosomes from their equilibrium positions. Furthermore, for repetitive DNA sequences, such as telomeres, we find thermal ratchets that propel nucleosomes in a preferred direction.

I. INTRODUCTION

Molecular motors transform chemical energy into mechanical energy which is used to perform a number of actions inside the cell: the transport of cargo by kinesin, dynein, or myosin motors has received ample attention in the statistical mechanics and biophysics communities; a recent review is Ref. [1]. Somewhat less studied, molecular motors also act at the level of DNA, notably as helicases that are small motors opening up the DNA double strand [2]. Even less studied are the so-called chromatin remodelers that regulate the positions of nucleosomes [DNA-protein complexes where 150 base pairs (BPs) are wrapped in almost two turns around an octamer of histone proteins] in chromatin; in the above-mentioned review [1] they appear in the Abstract only to be never mentioned again.

Chromatin remodelers are classified in four families, based on their sequence homology [3]. As far as their motor domain is concerned, it in fact derived from helicases: chromatin remodelers have evolved from motors that separate the two strands of DNA to motors that can separate the DNA strand from the histone octamer, either in order to remove the histone proteins altogether, or to displace the octamer along the DNA molecules to render the underlying DNA sequence accessible.

Statistical physics based models for chromatin remodelers are still rare, and often directed linked to *in vitro* experiments; see, e.g., Refs. [4,5]. Recent structural insights in

the functioning of remodelers, and also first coarse-grained simulations developed on the basis of experimental insights [6], allow us to push this development further, which is what we present in this paper. We develop a model for the action of the chromatin remodeler acting on nucleosomes moving in a sequence-dependent potential—a key feature entirely missing from earlier work, however of clear biological relevance since remodelers shift nucleosomes away from their intrinsically preferred locations in a sequence dependent manner [7–9]. Our model description allows us to compare the diffusive mode of nucleosomes to the chromatin remodeler-dependent displacement of nucleosomes along DNA.

II. METHODS

A. A basic mechanochemical cycle for chromatin remodeling

In a nucleosome a persistence length of DNA of about 150 BPs is wrapped nearly twice around the histone octamer, leading to a substantial DNA bending energy [10]. As the shape and elasticity of the DNA double helix depend on the underlying BP sequence [11], this energy is sequence dependent, leading to a position dependent energy landscape for nucleosomes [12–15]. However, in the absence of active processes, nucleosome repositioning occurs extremely slowly [16,17]. In fact, *in vivo*, nucleosomes are repositioned by chromatin remodelers [18,19]. This active process might speed up the equilibration of the system, as suggested in Ref. [20], but can also drive it further away from it, e.g., when it causes accumulation of nucleosomes close to promoters [7]. The resulting density distribution of the nucleosomes along the DNA is biologically relevant because it has profound implications for the accessibility to genetic information [10].
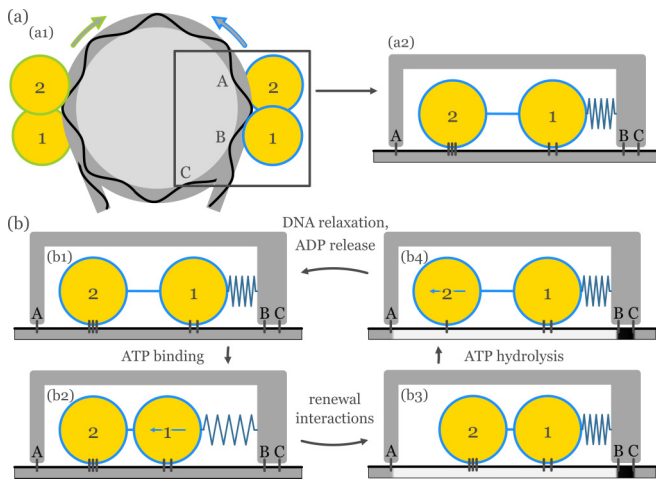
FIG. 1. (a1) Sketch of a nucleosome (DNA, dark gray; octamer, light gray) and a remodeler made from two lobes ("1" and "2") bound at two possible locations (green and blue). The induced sliding directions (arrows) depend on the remodeler position. (a2) Mapping of the relevant subsystem onto a molecular motor in a box. The box, representing the octamer, gives the remodeler limited space and is bound to the DNA (black line) at three sites, A, B, and C. (b) The mechanochemical cycle of the motor-in-a-box model.

We follow the coarse-grained simulations of Ref. [6] which puts forward a plausible scenario of remodeler action on nucleosomes, and first build a one-dimensional model of a remodeler acting on a nucleosome. Figure 1(a1) shows the remodeler which contains two lobes, sketched as pairs of yellow disks, bound to a nucleosome (shown in two gray scales) at the two possible positions (blue and green outlines) with the resulting repositioning directions (arrows) in each case. The mapping of the three-dimensional system to a one-dimensional model is depicted in Fig. 1(a2). The gray box represents the confined space for the remodeler lobes (the yellow circles) which results from the three-dimensional structure of the nucleosome [6]. Dark gray lines represent binding sites of the remodeler lobes 1 and 2 and the nucleosomal DNA, and between the nucleosomal DNA and the histone core (labeled A, B, and C). An electrostatic attraction between lobe 1 and the opposite DNA gyre [6] is indicated by a blue spring. In order to keep the schematic image compact, we depict sites B and C close together, although they are the same distance apart as the sites A and B.

The one-dimensional model can be used to explain how the mechanochemical cycle of the remodeler causes nucleosome repositioning, Fig. 1(b). ATP binding induces a conformational change of the remodeler lobes from an open, Fig. 1(b1), to a closed conformation, Fig. 1(b2), with the motion of lobe 1 towards lobe 2, due to the weaker DNA contacts of the former. Through the repositioning of the remodeler lobe 1, the "original" interaction of this lobe with the nucleosome is disturbed, represented by the stretched blue spring. The renewal of these interactions, Fig. 1(b3), leads to a movement of both remodeler lobes which deforms the bound DNA. Specifically, the binding point B of the DNA with the histone core is opened and then closed at a different BP position. This results in two highly deformed DNA sections, a stretched overtwisted (white

color) and a compressed undertwisted (black color) section, each between two binding points of the DNA to the histone core. Experiments [21–23] indeed show that at least some of the remodelers induce such twist defects in the wrapped DNA. Then ATP hydrolysis weakens the remodeler lobe 2 DNA contact and induces opening via the motion of this lobe away from the other lobe, Fig. 1(b4). ADP release and DNA relaxation complete the cycle. The relaxation is done by the opening and closing of the binding points A and C by thermal fluctuations and the release of the stretched and compressed DNA to the outer nucleosomal DNA ends where they eventually leave the nucleosome. In the end, both remodeler lobes have returned to their starting conformation, but the nucleosome has moved by one BP and the cycle can start again.

Zooming out again to the full system of Fig. 1(a1), we find the nucleosome transformed into a self-propelled particle by the binding of a remodeler with a direction of motion that depends on the binding position. As the movement requires the local deformation of DNA in the form of a pair of twist defects and as the deformation energy depends on the local BP sequence (which, for a given nucleosome position, is different for the two remodeler binding positions), we expect a system where the stepping rates to the left and right are different and essentially independent from each other. We now introduce a general framework to describe this type of system and highlight some typical features.

B. General framework

We consider a particle on a one-dimensional track that jumps to neighboring positions with a rate that depends on the particle's position and jump direction. We assume that the rates for the two jump directions are independent, which amounts to breaking detailed balance. We relate each jumping rate to energy barriers E by a Boltzmann factor $e^{-\beta E}$ with β denoting an inverse (effective) temperature. This produces two sets of energy barriers, for jumps to the left and to the right, which we interpret as two different energy landscapes V_l and V_r for the two jumping directions. The probability density Ψ of the particle at position x and time t evolves then according to the discrete master equation:

$$
\begin{aligned}
\Psi(x, t + \Delta t) - \Psi(x, t) &= e^{-\beta V_l(x+\Delta x)}\Psi(x + \Delta x, t) \\
&+ e^{-\beta V_r(x-\Delta x)}\Psi(x - \Delta x, t) \\
&- e^{-\beta V_l(x)}\Psi(x, t) \\
&- e^{-\beta V_r(x)}\Psi(x, t),
\end{aligned}
\tag{1}
$$

where Δx denotes the jump length. The steady-state solution

$$
\lim_{t \to \infty} \Psi(x, t) = p(x)
\tag{2}
$$

depends on the values of V_l and V_r, especially on their relative sizes. For example, for $V_l < V_r$ the particle jumps more likely to the left. At positions where V_l and V_r cross, the behavior of the particle changes as shown in Fig. 2(a), where the blue and green lines represent the potentials for jumps to the left and right. At the left intersection, $x = 1/4$, the particle is pushed on average toward the crossing point, whereas at the right intersection, $x = 3/4$, it is pushed away from it, leading to a maximum of p at $x = 1/4$ and a minimum at $x = 3/4$.
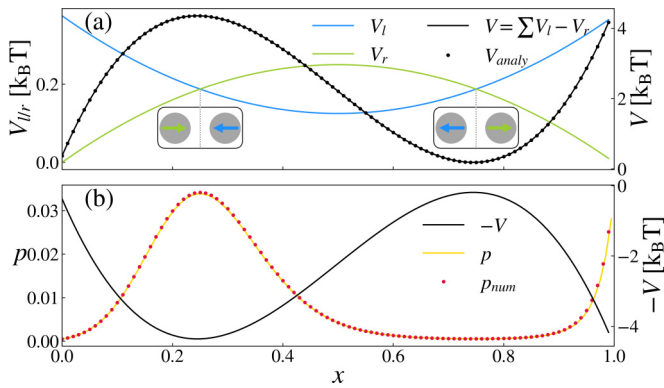
FIG. 2. (a) The energy landscapes for jumping to the left (blue) and right (green) leading to the effective potential V in Eq. (3) (black curve/dots). Extremal points of V occur at intersections of V_l and V_r where the preferred direction of motion of the particle changes (see illustrations inside the boxes). (b) Probability density distribution p for the steady state: approximate solution Eq. (3) (yellow line) and numerical solution (red dots). We use $\beta = 1$.

In general, intersections of V_l and V_r act as repellers and attractors of particles, leading to extremal points of p. This can be seen by inspecting p, shown as red dots in Fig. 2(b), which is obtained from the numerical solution of the master Eq. (1).

We note that the master Eq. (1) can be approximated by a drift diffusion Eq. [24] where the drift term $\partial_x[(e^{-\beta V_l} - e^{-\beta V_r})\Psi]$ can be linearized to $\beta\partial_x(V_r - V_l)\Psi$ if $\beta V_{l/r} < 1$. This suggests that the probability density distribution p can be approximated by

$$p(x) = \frac{1}{N}e^{\beta V(x)} = \frac{1}{N}e^{\beta \sum_{y=0}^{x}[V_l(y)-V_r(y)]}, \tag{3}$$

where N denotes a normalization factor. The function V is shown as a black curve in Fig. 2 [25]. Equation (3) is not the exact steady-state solution of the master Eq. (1), but is expected to be a good approximation in the limit of slowly varying continuous energy landscape functions V, V_l, and V_r. For example, in Fig. 2(b) Eq. (3) is represented by the yellow line and is indeed in excellent agreement with the numerical solution (red dots).

Of special interest is the case when the two energy landscapes V_l and V_r are periodic. Figure 3(a) shows potentials with linear decreasing and increasing sections, e.g., $V_{l/r} \sim \pm x$, but for one potential the increasing parts are slightly nonlinear: $V_{l/r} \sim x^\alpha$ with $\alpha = 1.0, 1.1, \ldots, 1.5$. The flux in a system with periodic boundary conditions,

$$J(x) = e^{-\beta V_r(x)}p(x) - e^{-\beta V_l(x+\Delta x)}p(x+\Delta x), \tag{4}$$

is shown Fig. 3(b). Starting from the symmetric case, $\alpha = 1$, without flux, the magnitude of J increases as α moves away from this value. The direction of the flux is related to the sum of the energy expenditure for the movement over one period, $\sum V_{l/r}$. Systems where particles move in preferred directions in a periodic potential have been invoked in models for molecular motors themselves [26–29] but here this so-called ratchet effect appears on a higher level through the action of a motor that binds to a particle at two different positions.
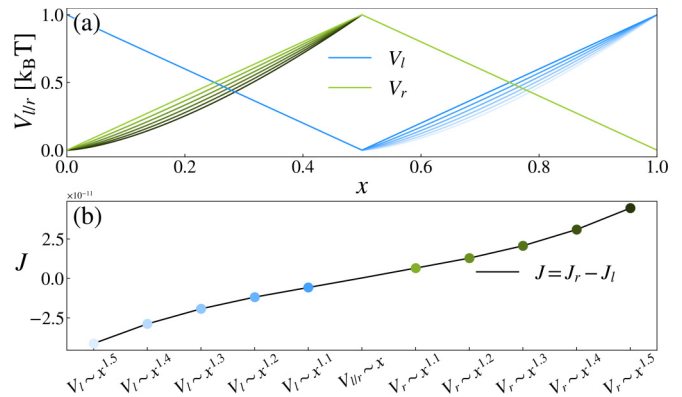

FIG. 3. Flux in ratchets: (a) set of periodic potentials V_l and V_r with increasing left-right asymmetry and (b) the corresponding increasing flux. We use $\beta = 1$.

C. Parametrizing the model

We now estimate the potentials V_l and V_r by building a coarse-grained model of a chromatin remodeler. The DNA is represented by a bead-spring chain which interacts with other components representing the protein core and the remodeler. The springs account for the sequence-dependent elasticity and geometry of the DNA double helix and are parametrized by the rigid base pair model [11]. The chain is 20 springs long, corresponding to the 20 BP DNA stretch which is in contact with the remodeler. Figure 4(a) shows the schematic representation of the remodeler at the two possible positions on the nucleosomal DNA and Fig. 4(b) shows the detailed microscopic representation of one of the remodeler-DNA complexes. We assume that the rate-limiting process in a successful defect pair formation is the thermally induced crossing of the energy barrier between the states shown in Figs. 1(b2) and 1(b3) whereas ATP hydrolysis takes place instantaneously afterwards. In the detailed model this means to go from the top to the bottom state in Fig. 4(b).
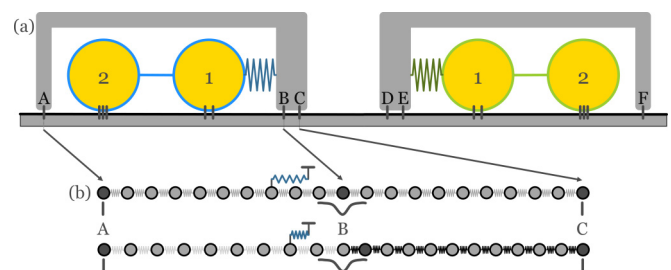

FIG. 4. (a) Motor in a box at its two possible positions (see also Fig. 1). Between the binding sites of the DNA to the protein core, labeled A to F, are always ten BPs. (b) Detailed view for one of the motor positions. DNA is modeled as a bead-spring chain where the spring parameters depend on the involved BP step. The blue spring represents the electrostatic interaction of lobe 1 with the nucleosome. Top: Nucleosomal DNA in relaxed state with ten BPs each between binding points A and B and between B and C. Bottom: Twist defect with a compressed DNA section with 11 BP steps between B and C (darker color of springs) and a stretched section with nine BP steps between A and B (lighter color).

Note that even though the motor positions for the two directions are 30 BPs apart (see Fig. 4) V_l is not a shifted copy of V_r: the remodeler points in opposite directions at the two binding positions and thus deforms the involved DNA stretch differently. Here we focus on a twist defect pair which causes a motion of the nucleosome to the left side. The calculation for the other direction follows from the symmetry of the system.

Figure 4(b) shows the involved 21 BPs without (top) and with the twist defect (bottom). In the absence of the defect, the BPs are equally distributed between the binding sites of the DNA to the histone octamer and the first, tenth, and last (20th) BPs are bound to the histone octamer at points A, B, and C, with the bound beads shown in darker gray. When the twist defect pair is present, there is a stretched part with only nine BP steps and a compressed part with 11 BP steps [see bottom of Fig. 4(b)]. The twist defect pair is caused by the movement of the tenth BP to the right side and the successive binding of the ninth BP to B instead.

To calculate the energy landscape experienced by the system as the twist defect is introduced (and from this the energy barrier V_l), we minimize the energy of the system for every position of the ninth BP, starting with the relaxed system and ending with the system containing a twist defect pair. For simplicity we fix the total length of the chain of springs, by assuming the binding points A and C to constitute rigid constraints. We set the position of point A at $x_A = 0$ and of C at $x_C = 20\,l_{\mathrm{BP}}$ with l_{BP} being the typical BP step height, $l_{\mathrm{BP}} = 3.4$ Å. Only the binding point B is modeled as a potential well allowing the bound BP to change. The energy as a function of the positions of the BPs, $\vec{x}$, has then three contributions:

$$E(\vec{x}) = E_{\mathrm{int}}(\vec{x}) + E_{\mathrm{spring}}(\vec{x}) + E_{\mathrm{pot}}(\vec{x}) \tag{5}$$

with E_{int} representing the energy of the electrostatic spring (blue spring in Fig. 4), E_{spring} the deformation energy of the spring-bead chain, and E_{pot} the binding energy of BP 9 or 10 to site B.

According to Ref. [22], the electrostatic interaction between remodeler lobe 1 and the other coil of the wrapped DNA acts on the seventh BP when ATP is bound to the remodeler and to the eighth BP otherwise. We model this interaction as a spring, with spring constant K' and equilibrium length s_{eq}:

$$E_{\mathrm{int}}(x) = \tfrac{1}{2} K'(x - s_{\mathrm{eq}})^2, \tag{6}$$

where x is the position of BP 7. s_{eq} is chosen to be the length of the electrostatic spring for the relaxed chain of springs before ATP is bound, i.e., when lobe 1 interacts with BP 8. Upon ATP binding there is thus initially a mismatch between x, the position of BP 7, and s_{eq}. The electrostatic spring pulls the remodeler towards the right and helps in the creation of the twist defect pair. As discussed later, we choose $K' = K k_B T$ Å^{-2} with $K = 3$.

The deformation energy of the chain of springs is given by

$$E_{\mathrm{spring}}(x) = \frac{1}{2} \sum_{n=1}^{20} k_n (x - s_n)^2, \tag{7}$$

with k_n denoting the stiffness and s_n the equilibrium length of the nth spring. Both values depend on the chemical identify

of the involved BP step. Here we use the parameters derived from the rigid base pair model [11] for the spring constants and intrinsic lengths. This model describes every BP as a rigid body. The conformation of a given BP step is then described by the values of its six degrees of freedom (three translational and three rotational) which are the components of a six-component vector q. The associated elastic energy of that BP step is given by

$$E = \tfrac{1}{2}(q - q_0)M(q - q_0), \tag{8}$$

where q_0 denotes the intrinsic preferred values and M is a 6×6 stiffness matrix. The total elastic energy is then the sum of the energies of all BP steps. The rigid base pair model assumes thus only nearest-neighbor interactions with a quadratic deformation energy. Here we use only one component of q, called rise, which describes the stretching and compression of the contour length of the DNA double helix. This is the stiffest deformation mode involved in twist defect formation. The other relevant deformation mode, twist, is softer. Specifically, for a twist defect the cost in changing rise is about $1.37 k_B T$ (0.34 Å displacement, average stiffness $23.8 k_B T$ Å^{-2}) and the cost in changing twist is $0.38\,k_B T$ (3.6° extra twist, average stiffness $0.06 k_B T$ deg^{-2}), i.e., about three times smaller. Nondiagonal matrix elements of M, e.g., twist-rise coupling, are even about ten times smaller. Therefore, in Eq. (7), s_n denotes the rise of the nth BP step and k_n its elasticity. The rise-related parameters for all possible BP steps are provided in Table I.

Finally, we model the binding energy as follows:

$$E_{\mathrm{pot}}(x) = -U_0 \left[\left(\frac{x - 10\,l_{\mathrm{BP}}}{0.5\,l_{\mathrm{BP}}} \right)^2 - 1 \right]^2, \tag{9}$$

if $|x - 10\,l_{\mathrm{BP}}| < 0.5\,l_{\mathrm{BP}}$, and zero otherwise. x is here either the position of BP 9 or 10, whichever is within the range of binding site B. The potential well has a depth $U_0 = 12 k_B T$ and width l_{BP} and is centered at $10\,l_{\mathrm{BP}}$; see Ref. [30] for an estimation of these values.

III. RESULTS

A. Energy landscapes of chromatin remodeler action

We calculate the energy landscape for the formation of a twist defect pair as a function of the position of the ninth BP. For this we equilibrate the positions of all the beads under the constraints that the total length of the chain is constant and that the position of BP 9 is fixed. This is done by numerically determining the total energy minimum of Eq. (5) as a function of two parameters only: the positions of BPs 7 and 10. These are sufficient as they form the end points of four effective springs: from the left end to BP 7, from BP 7 to BP 9, from BP 9 to BP 10, and from BP 10 to the end. Note that these effective springs could not be constructed so easily if we would also account for the twist and twist-rise coupling energies. The thick curves in Fig. 5 show the energy landscapes for four different BP sequences. The curves are qualitatively similar: With rising displacement Δx of BP 9, the energy increases until a maximum is reached. Beyond that point a local minimum occurs, before the energy rises again. Note that the resulting energy barriers show a substantial dependence on

TABLE I. Rise parameters of the rigid base pair model [11].

	AA/TT	AT	AC/GT	AG/CT	TA	TC/GA	TG/CA	CC/GG	CG	GC
x_{rise} (Å)	3.27	3.31	3.36	3.34	3.42	3.37	3.33	3.42	3.39	3.40
k_{rise} ($k_B T$ Å^{-2})	21.75	25.55	23.86	29.50	21.91	22.82	18.24	30.31	14.16	25.86

the underlying BP sequence. For the four example cases they range from $9.6 k_B T$ to $15.6 k_B T$.

The plots show also the three individual contributions to the total energy, given in Eq. (5). The blue lines in Fig. 5 represent the energy from the electrostatic spring which tends to zero with increasing Δx, as the interaction between remodeler lobe 1 and the other DNA gyre is reestablished. The light gray lines give the elastic energy inside the chain of springs and show the opposite behavior: an overall increase of E_{spring} with Δx with a small drop in energy around $\Delta x = 2$ Å. Before this drop, the increase in energy is almost exclusively concerning the first ten springs as BP 10 remains bound at B. The local drop occurs when the tension between BPs 9 and 10 is so high that BP 10 is pushed out of the potential well of the binding site. This can be best seen by inspecting the third contribution, E_{pot}, which shows a sharp increase as the tenth BP leaves the well. At the same time, there is a drop in E_{spring}. As BP 9 is pushed further to the right, it enters the potential well, causing,

together with the contribution from the electrostatic spring, the local minimum in the total energy. In general, we observe that the point where the bound BP changes corresponds to the location of the local energy maximum causing the energy barrier ΔE for the creation of the twist defects.

B. Remodeler-induced nucleosome positioning

From the values of ΔE at the various positions of the remodeler on the DNA we can calculate the energy landscape V_l and V_r. Using a randomly picked 300 BP stretch from *S. cerevisiae* [31], we calculate V_l, V_r, and V and find that V shows an undulating landscape with various local minima and maxima [see top diagram of Fig. 6(a)]. The bottom diagram presents the steady-state solution p which features a strong peak in the middle of the BP stretch and two minor local maxima to the right. This is an example of remodeler-induced nucleosome positioning.

For the calculation of the energy barrier we set so far the parameter K to 3. However, the strength of the interaction of remodeler lobe 1 with the other DNA gyre is not known. We therefore examine the influence of this parameter on the energy landscapes in Fig. 7, which are presented together
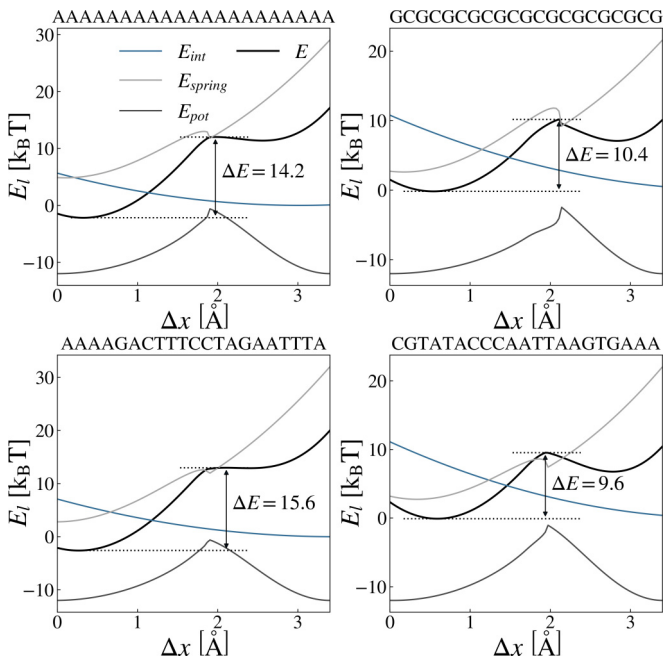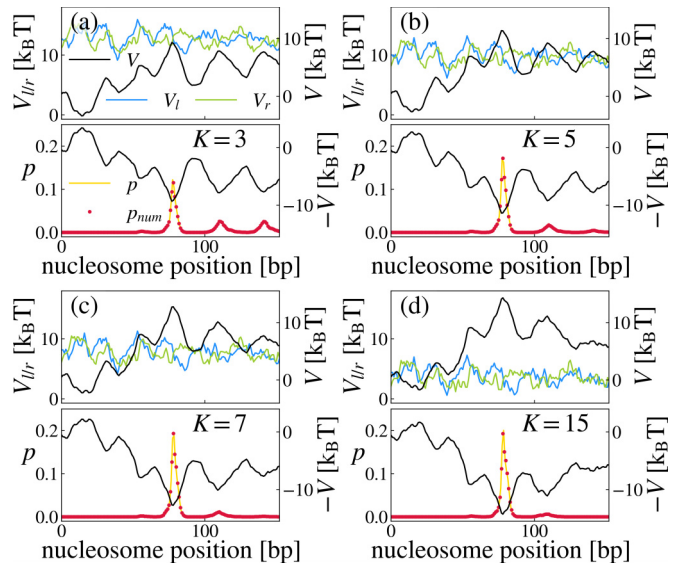

FIG. 5. Energy barrier for twist defect pair formation for different BP sequences (indicated on the top of the diagrams). Black curves show the energy landscapes of the system as a function of the displacement Δx of the ninth BP towards the center of the chain. The energies are composed of the electrostatic interaction of remodeler lobe 1 with the other DNA turn, Eq. (6) (blue curves), the energies resulting from the stretching and compression of the DNA, Eq. (7) (light gray curves), and the energies from the binding of the DNA with the histone core at site B, Eq. (9) (dark gray curves). Here we use $K = 3$ for the (dimensionless) spring constant.

FIG. 6. Sequence-dependent nucleosome positioning caused by the sequence-dependent remodeler action for different stiffnesses K of the "electrostatic spring." For each K value, the top diagram shows the potentials V_l (blue), V_r (green), and V (black) for a 300 BP stretch of gene YAL002W of *S. cerevisiae*. The bottom diagram presents the numerical steady-state solution p, Eq. (3), as red dots and the analytical solution as a yellow curve together with the potential $-V$ (black curves). Throughout we use $\beta = \frac{1}{4}$.
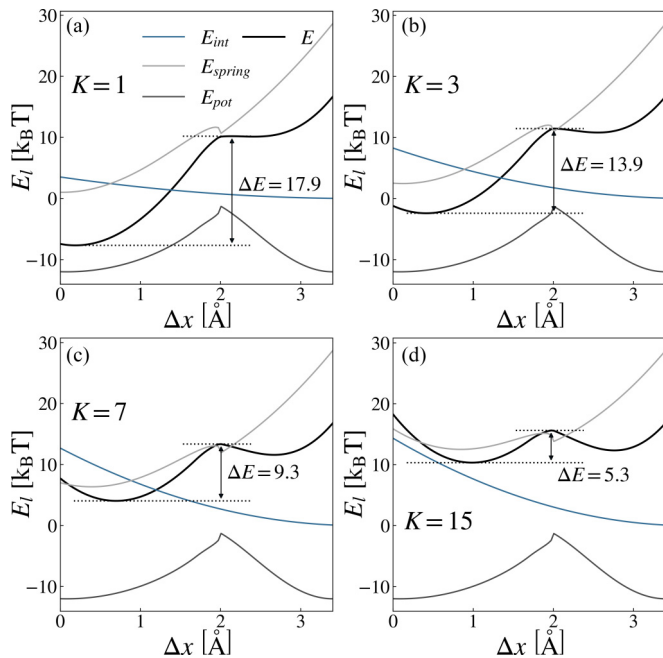
FIG. 7. Energy barrier for twist defect pair formation for a 20 BP stretch of gene YAL002W for different stiffnesses K of the electrostatic spring. Curves are depicted as in Fig. 5. (a) $K = 1$, (b) $K = 3$, (c) $K = 7$, and (d) $K = 15$. Throughout we use the sequence ATGGAGCAAAATGGCCTTGA.
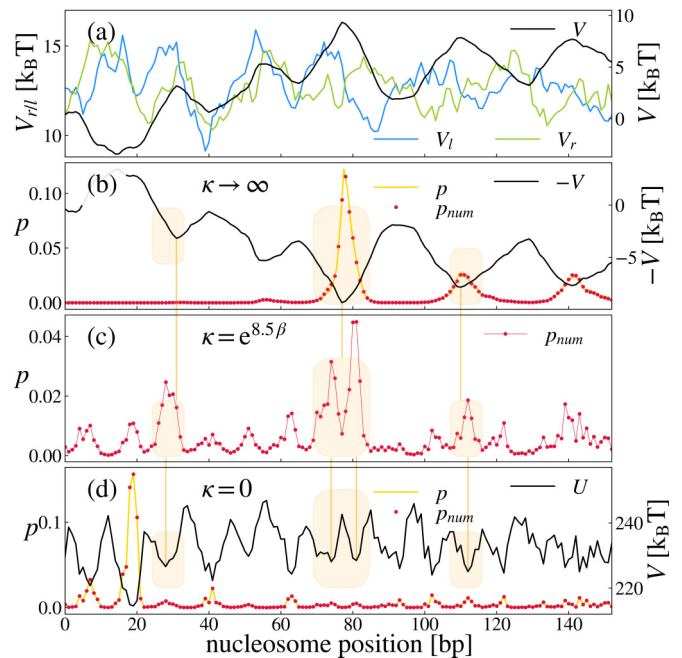

FIG. 8. Sequence-dependent nucleosome positioning. (a) Potentials V_l (blue), V_r (green), and V (black) for a 300 BP stretch of gene YAL002W of *S. cerevisiae*. (b–d) Numerical steady-state solution p of Eq. (10) for (b) dominant remodeler action, $\kappa \to \infty$, (c) a mixed situation, and (d) pure diffusion, $\kappa = 0$. In the limiting cases, analytical solutions are also provided (yellow) together with the potentials $-V$ and U (black). Orange boxes highlight maxima in the mixed phase (c) which occur where both U and $-V$ show minima. We use $\beta = \frac{1}{4}$, $K = 3$.

with their three components for four different values of K: 1, 3, 7, and 15. The binding energy E_{pot} shows hardly any K dependence. The interaction energy E_{int}, which is proportional to K, starts from larger values for $\Delta x = 0$ and thus goes more steeply down towards $E_{int} = 0$ at $\Delta x = 3.4$ Å. Remarkably, the increase in stiffness of the electrostatic spring has a strong effect on E_{spring}. This is caused by the seventh BP being increasingly pushed towards the ninth BP whose position is set to a given Δx value. The strong deformation in the chain of springs up to the ninth BP for small Δx values leads to an overall slower increase of E_{spring} for larger K values. Being the sum of these three contributions, the overall energy shows more and more the shape of a double well potential. As the minimum for small displacements gets lifted up with increasing K, the height of the energy barrier goes down.

Despite these changes, the resulting probability distribution p for the nucleosome probability distribution remains remarkably unaffected by the choice of K (see Fig. 6). The main effect of increasing K is a shift of V_l (blue) and V_r (green) to smaller values, as we have already observed in Fig. 7. The shapes of the landscapes remain similar and also the crossing points of V_l and V_r occur at the same positions. This is also visible when inspecting the shape of the potential V (black). As a result, the density distributions for the nucleosome positioning all look very similar. Especially, as the minimum of V is always located at the same position (shown here in the middle of the graphs), the maximum of p is always at that position too. It is a lucky coincidence that the value of the parameter we have not yet been able to extract from experimental data has only a small effect on the results which we present in this paper.

C. Active vs passive nucleosome positioning

As mentioned in the the Methods section, nucleosomes also reposition themselves autonomously through nucleosome sliding, resulting in a probability density that reflects the sequence-dependent bending energy U of the nucleosomal DNA. U is calculated from our previous probabilistic nucleosome positioning model, also based on the rigid base pair model [32,33]. The full master equation

$$\Psi(x, t + \Delta t) - \Psi(x, t) = \pm \kappa e^{-\beta V_{l/r}(x_0)} \Psi(x_0, t)$$
$$\pm e^{-\beta \Theta[U(x_{end}) - U(x_0)][U(x_{end}) - U(x_0)]}$$
$$\times \Psi(x_0, t) \qquad (10)$$

accounts for both processes, with Θ the Heaviside step function. There are four possible jumps involving position x (from x_0 to x_{end}) in two different ways, passive (second line) and active (first line). The parameter κ represents the relative strength of the action of the chromatin remodeler compared to the diffusion. It can be interpreted as the parameter which controls the time scales between jumps via diffusion and through the action of the chromatin remodeler.

The steady-state solution for dominant chromatin remodeler action, $\kappa \to \infty$, is given by Eq. (3) and is shown in Fig. 8(b). As expected, maxima occur at minima of $-V$. The opposite limit, $\kappa \to 0$, leads to the Boltzmann distribution $p(x) = e^{-\beta U(x)}$ [see Fig. 8(d)]. Importantly, the two sequence-dependent potential V in Fig. 8(b) and U in Fig. 8(d)
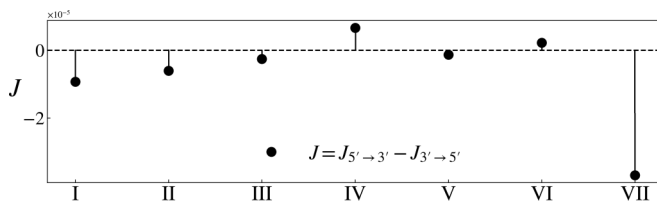
FIG. 9. Fluxes along different telomeric sequences in a system with periodic boundaries. Positive (negative) values correspond to outward (inward) fluxes on the chromosome. We use $\beta = \frac{1}{4}$, $K = 3$. I, vertebrates; II, insects and butterflies; III, gill-foot crabs and tubeworms; IV, ciliates; V, higher plants; VI, green algae; VII, schizosaccharomyces.

are essentially unrelated, as V reflects the overstretching and compression of the involved 20 BPs whereas U represents the bending energy of the full 150 BPs. Thus the resulting nucleosome probability densities in Figs. 8(b) and 8(d) peak at unrelated positions. Between these two asymptotic regimes both potentials contribute to p. In Fig. 8(c) we chose $\kappa = e^{8.5\beta}$ which results in the same order of magnitude for the diffusion and remodeling terms. In this case the maxima in the probability density are located, where minima in *both* potentials occur, highlighted by the orange boxes.

The specific example shown in Fig. 8 suggests that the remodeler can act as a switch, moving the nucleosome from BP position 19 in its absence, Fig. 8(d), to BP position 78, Fig. 8(b). The idea of nucleosome switches has been put forward earlier as a result of frustration between packing effects of multiple nucleosomes and the sequence-dependent nucleosomal potential energy landscape [34]. However, in our scenario, this effect can occur even for a single nucleosome, as the effective energy landscape it experiences changes shape in the presence of active remodeling.

D. Repositioning on telomeric sequences

Finally, we return to the ratchet effect, discussed earlier and shown in Fig. 3, and study its consequences for nucleosome repositioning on the periodic BP sequences of telomeric repeats (e.g., in vertebrates these are six BP repeats). Figure 9 shows the predicted fluxes on telomeres for different groups of organisms [35]. The fluxes differ greatly in magnitude and even show opposite signs. Whereas vertebrate telomeres, for example, induce a small inward flux (towards the centromere), the ones for ciliates cause an outward flux (toward the telomeric ends). Whether such fluxes occur *in vivo* remains unclear but they might have biological implications by, e.g., creating compressive forces on telomeric nucleosomal arrays.

IV. CONCLUSION

Based on insights gained from recent experiments and simulations, we have put forward a model of chromatin remodeling motors and employed it to study the active repositioning of a nucleosome. Remodelers can drive the nucleosome in either direction along the DNA depending on its binding position on the nucleosome. We have calculated the probability density of the nucleosome along DNA as a result of active repositioning. A key finding is that the remodeler pushes the nucleosome to certain locations on the DNA and away from others, and that these preferences are not determined by the intrinsic sequence preferences of nucleosomes. Inspired by the idea of a "genomic code for nucleosome positioning" [12] resulting from thermal equilibration, we speculate that there might be a "genomic code for nucleosome remodeling" instead, i.e., BP sequences may have evolved to create attractors, repellers, or even ratchets for remodeler-propelled nucleosomes.

[1] M. L. Mugnai, C. Hyeon, M. Hinczewski, and D. Thirumalai, Theoretical perspectives on biological machines, Rev. Mod. Phys. **92**, 025001 (2020).

[2] *DNA Helicases and DNA Motor Proteins*, 1st ed., edited by M. Spiess (Springer, New York, 2012).

[3] C. R. Clapier and B. R. Cairns, The biology of chromatin remodeling complexes, Annu. Rev. Biochem. **78**, 273 (2009).

[4] Y. Vandecan and R. Blossey, Stochastic description of single nucleosome repositioning by ACF remodelers, Phys. Rev. E **85**, 061920 (2012).

[5] Y. Vandecan and R. Blossey, Fokker-Planck description of single nucleosome repositioning by dimeric chromatin remodelers, Phys. Rev. E **88**, 012728 (2013).

[6] G. B. Brandani and S. Takada, Chromatin remodelers couple inchworm motion with twist-defect formation to slide nucleosomal DNA, PLoS Comput. Biol. **14**, e1006512 (2018).

[7] N. Krietenstein, M. Wal, S. Watanabe, B. Park, C. L. Peterson, B. F. Pugh, and P. Korber, Genomic nucleosome organization reconstituted with pure proteins, Cell **167**, 709 (2016).

[8] Y. Lorch, B. Maier-Davis, and R. D. Kornberg, Role of DNA sequence in chromatin remodeling and the formation of nucleosome-free regions, Genes Dev. **28**, 2492 (2014).

[9] J. Winger and G. D. Bowman, The sequence of nucleosomal DNA modulates sliding by the Chd1 chromatin remodeler, J. Mol. Biol. **429**, 808 (2017).

[10] H. Schiessel, Spatial and temporal organization of chromatin at small and large scales, Annu. Rev. Condens. Matter Phys. **14**, 193 (2023).

[11] W. K. Olson, A. A. Gorin, X.-J. Lu, L. M. Hock, and V. B. Zhurkin, DNA sequence-dependent deformability deduced from protein-DNA crystal complexes, Proc. Natl. Acad. Sci. USA **95**, 11163 (1998).

[12] E. Segal, Y. Fondufe-Mittendorf, L. Chen, A. Thåström, Y. Field, I. K. Moore, J.-P. Z. Wang, and J. Widom, A genomic code for nucleosome positioning, Nature (London) **442**, 772 (2006).

[13] M. Zuiddam, R. Everaers, and H. Schiessel, Physics behind the mechanical nucleosome positioning code, Phys. Rev. E **96**, 052412 (2017).

[14] J. Neipel, G. Brandani, and H. Schiessel, Translational nucleosome positioning: A computational study, Phys. Rev. E **101**, 022405 (2020).

[15] A. Basu, D. G. Bobrovnikov, Z. Qureshi, T. Kayikcioglu, T. T. M. Ngo, A. Ranjan, S. Eustermann, B. Cieza, M. T. Morgan, M. Hejna, H. T. Rube, K.-P. Hopfner, C. Wolberger, J. S. Song, and T. Ha, Measuring DNA mechanics on the genome scale, Nature (London) **589**, 462 (2021).

[16] G. Meersseman, S. Pennings, and E. M. Bradbury, Mobile nucleosomes: A general behavior, EMBO J. **11**, 2951 (1992).

[17] I. M. Kulić and H. Schiessel, Chromatin dynamics: Nucleosomes go mobile through twist defects, Phys. Rev. Lett. **91**, 148103 (2003).

[18] R. Blossey and H. Schiessel, The latest twists in chromatin remodeling, Biophys. J. **114**, 2255 (2018).

[19] I. M. Nodelman and G. D. Bowman, Biophysics of chromatin remodeling, Annu. Rev. Biophys. **50**, 73 (2021).

[20] E. Segal and J. Widom, What controls nucleosome positions? Trends Genet. **25**, 335 (2009).

[21] J. Winger, I. M. Nodelman, R. F. Levendosky, and G. D. Bowman, A twist defect mechanism for ATP-dependent translocation of nucleosomal DNA, eLife **7**, e34100 (2018).

[22] M. Li, X. Xia, Y. Tian, Q. Jia, X. Liu, Y. Lu, M. Li, X. Li, and Z. Chen, Mechanism of DNA translocation underlying chromatin remodelling by Snf2, Nature (London) **567**, 409 (2019).

[23] A. Sabantsev, R. F. Levendosky, X. Zhuang, G. D. Bowman, and S. Deindl, Direct observation of coordinated DNA movements on the nucleosome during chromatin remodelling, Nat. Commun. **10**, 1720 (2019).

[24] M. V. Smoluchowski, Über brownsche molekularbewegung unter einwirkung äußerer kräfte und deren zusammenhang mit der verallgemeinerten diffusionsgleichung, Ann. Phys. (Leipzig) **353**, 1103 (1916).

[25] In this example we used $V_l = (x - 1/2)^2 + 1/8$ and $V_r = -(x - 1/2)^2 + 1/4$ which results in $V(x) = \frac{2n}{3}x^3 + (1 - n)x^2 + (\frac{1}{3n} - 1 + \frac{3n}{8})x + \frac{3}{8}$ with n the number of steps.

[26] M. O. Magnasco, Forced thermal ratchets, Phys. Rev. Lett. **71**, 1477 (1993).

[27] F. Jülicher, A. Ajdari, and J. Prost, Modeling molecular motors, Rev. Mod. Phys. **69**, 1269 (1997).

[28] P. Reimann, Brownian motors: Noisy transport far from equilibrium, Phys. Rep. **361**, 57 (2002).

[29] I. M. Kulić, R. Thaokar, and H. Schiessel, Twirling DNA rings: Swimming nanomotors ready for a kickstart, Europhys. Lett. **72**, 527533 (2005).

[30] H. Schiessel, *Biophysics for Beginners: A Journey through the Cell Nucleus*, 2nd ed. (Jenny Stanford, New York, 2021).

[31] 300 bp stretch of YAL002W of *S. cerevisiae*: ATGGA GCAAA ATGGC CTTGA CCACG ACAGC AGATC TAGCA TCGAT ACGAC TATTA ATGAC ACTCA AAAGA CTTTC CTAGA ATTTA GATCG TATAC CCAAT TAAGT GAAAA ACTGG CATCT AGTTC TTCAT ATACG GCACC TCCCC TGAAC GAAGA TGGTC CTAAA GGGGT AGCTT CTGCA GTGTC ACAAG GCTCC GAATC CGTAG TCTCA TGGAC AACTT TAACA CACGT ATATT CCATC CTGGG TGCTT ATGGA GGGCC CACGT GCTTG TATCC GACAG CCACG TATTT TTTGA TGGGC.

[32] M. Tompitak, G. T. Barkema, and H. Schiessel, Benchmarking and refining probability-based models for nucleosome-DNA interaction, BMC Bioinf. **18**, 157 (2017).

[33] M. Tompitak, C. Vaillant, and H. Schiessel, Genomes of multicellular organisms have evolved to attract nucleosomes to promoter regions, Biophys. J. **112**, 505 (2017).

[34] D. J. Schwab, R. F. Bruinsma, J. Rudnick, and J. Widom, Nucleosome switches, Phys. Rev. Lett. **100**, 228105 (2008).

[35] I, vertebrates: TTAGGG. II, insects and butterflies: TTAGG. III, gill-foot crabs and tubeworms: TTAGGC. IV, ciliates: TTGGGG. V, higher plants: TTTAGGG. VI, green algae: TTTTAGGG. VII, schizosaccharomyces: TTACACG.